Iodine-enhanced Liver Vessel Segmentation in Photon Counting Detector-based Computed Tomography using Deep Learning

Sumin Baek[a], Okkyun Lee*[a], and Donghye Ye*[b]

[a]The Department of Robotics and Mechatronics Engineering, Daegu Gyeongbuk Institute of Science and Technology, Daegu, 42988 Korea
[b]The Department of Electrical and Computer Engineering, Marquette University, Milwaukee, WI, 53233 United States

ABSTRACT

Liver vessel segmentation is important in diagnosing and treating liver diseases. Iodine-based contrast agents are typically used to improve liver vessel segmentation by enhancing vascular structure contrast. However, conventional computed tomography (CT) is still limited with low contrast due to energy-integrating detectors. Photon counting detector-based computed tomography (PCD-CT) shows the high vascular structure contrast in CT images using multi-energy information, thereby allowing accurate liver vessel segmentation. In this paper, we propose a deep learning-based liver vessel segmentation method which takes advantages of the multi-energy information from PCD-CT. We develop a 3D UNet to segment vascular structures within the liver from 4 multi-energy bin images which separates iodine contrast agents. The experimental results on simulated abdominal phantom dataset demonstrated that our proposed method for the PCD-CT outperformed the standard deep learning segmentation method with conventional CT in terms of dice overlap score and 3D vascular structure visualization.

Keywords: Photon Counting Detector, Computed Tomography, Liver Vessel Segmentation, Deep Learning

1. INTRODUCTION

Vascular structures segmentation within the liver plays an important role in diagnosing and treating the patient's liver condition. For example, if there is a tumor in the patient's liver, determining the location of the tumor and the distribution of vascular structures in the liver before making liver resection will help planning for liver surgery.[1,2] In particular, visualizing blood vessels in three dimensions before radio frequency ablation treatments or minimally invasive surgery can provide a road map for analyzing the location of blood vessels related to lesions.[2] In addition, in the case of liver transplantation, the vascular structure of the liver donor can be identified in advance, helping to accurately verify whether it is suitable for liver donors.[3,4]

As such, the segmentation of the vascular structure in the liver is critical for the diagnosis and treatment of liver diseases. Liver vessel segmentation is challenging due to the anatomical variability of the structure of the liver and blood vessels. To facilitate the liver vessel segmentation, iodine-based contrast agents are usually injected into the patient to highlight the vascular structures in the liver. However, the contrast of the iodine-enhanced vessels to the surrounding tissue is limited in the conventional computed tomography (CT) with energy-integrating detectors.[5] Even though there are promising CT organ segmentation results using deep learning methods such as UNET,[6–8] it still remains challenging for deep learning methods to segment the liver vascular structures in the conventional CT images due to low contrast.

Further author information: (Send correspondence to Sumin Baek)
Sumin Baek: E-mail: bsk0610@dgist.ac.kr
Okkyun Lee: E-mail: oklee@dgist.ac.kr,
Donghye Ye: E-mail: donghye.ye@marquette.edu
*Corresponding author

7th International Conference on Image Formation in X-Ray Computed Tomography,
edited by Joseph Webster Stayman, Proc. of SPIE Vol. 12304, 1230432
 · 0277-786X · doi: 10.1117/12.2646541

Meanwhile, photon counting detector-based computed tomography (PCD-CT) is an emerging medical imaging technology, which has potential advantages over conventional CT. Especially, PCD-CT has the ability to enhance the contrast to noise ratio with iodine contrast agents, generate multi-energy images simultaneously, reduce the noise and increase the spatial resolution.[9] The degree of attenuation for each material by X-ray depends on the energy and properties of the material.[10] In particular, when the iodine is injected, the attenuation in the vessels increase, resulting in an energy-dependent difference in attenuation between the iodine-enhanced vessels and surrounding tissue in the liver. Thus, we hypothesize that the energy discrimination capability of the PCD-CT has benefit for the blood vessel segmentation compared to the conventional CT.

In this paper, we propose a 3D UNET for liver vessel segmentation in PCD-CT, which trains bin-wise images at once in a deep convolutional neural network with a single labeled image. We compare our proposed method with the same UNET structure trained by a conventional CT image (except the multi-channel input for the proposed one). Datasets are generated with abdominal simulation phantom with iodine-enhanced for the liver blood vessels. We apply a low concentration level of iodine, reducing the risk of contrast-induced nephropathy into a liver and vessel, with a relatively low level of iodine diffused in the liver.[11] The experimental results using the PCD-CT dataset are compared and analyzed with those using the conventional CT dataset through dice score and 3D vascular structure visualizations.

The paper is organized by the following. In Section 2, we describe the PCD-CT measurement models, and UNET architecture for liver vessel segmentation. Section 3 presents the experimental setup and the quantitative/qualitative assessment for liver vessel segmentation results with conventional CT and PCD-CT. The conclusion and discussion are provided in Section 4.

2. METHODS

Fig. 1 describes the overview of our liver vessel segmentation method using the PCD-CT. We first add the iodine on ground-truth 3D CT and generate 4-bin images based on the PCD-CT measurement model. We train the UNET from 3D random patches from 4-bin images and compare the liver vessel segmentation performance with the UNET trained on the corresponding conventional CT dataset.

2.1 PCD-CT measurement model

We assume that the bin-wise photon counts are independent Poisson random variables, and the expected counts $\bar{y}_b$ for the b-th energy bin of PCD-CT is given by

$$\bar{y}_b = \int_0^\infty I(E) S_b(E) e^{-\int \mu(r,E)dr} dE, \quad for\ b = 1, 2, \cdots, B, \tag{1}$$

where $I(E)$ represents the X-ray incident spectrum, and $S_b(E)$, which includes the spectral distortion in PCD, is a bin sensitivity function. $\int \mu(r, E)dr$ is the line integral of the linear attenuation coefficient.

An experiment was conducted using a conventional CT dataset as a comparison technique to the experiment using the PCD-CT dataset. We also assume that the measurement from the conventional CT, a single outcome from a detector, follows Poisson distribution, but with an expected counts $\bar{\lambda}$ as follows:

$$\bar{\lambda} = \int_0^\infty I(E) \left\{ \sum_{b=1}^{B} S_b(E) \right\} e^{-\int \mu(r,E)dr} dE, \tag{2}$$

For a given object, we use the measurements models of (1) and (2) to generate data sets for the PCD-CT and the conventional one, respectively. We applied filtered backprojection (FBP) with Shepp-Logan filter to the sinograms to obtain the data sets. Sample images of datasets for conventional CT and PCD-CT measurement models are shown in Fig. 1(c) and (d), respectively.

For the PCD-CT model, threshold values of energy bins set to the PCD are 20, 67, 101, 113 keV. An aluminium pre-filtered incident spectrum with 140kVp was used, and the total number of photons is $2.5\text{x}10^5$.

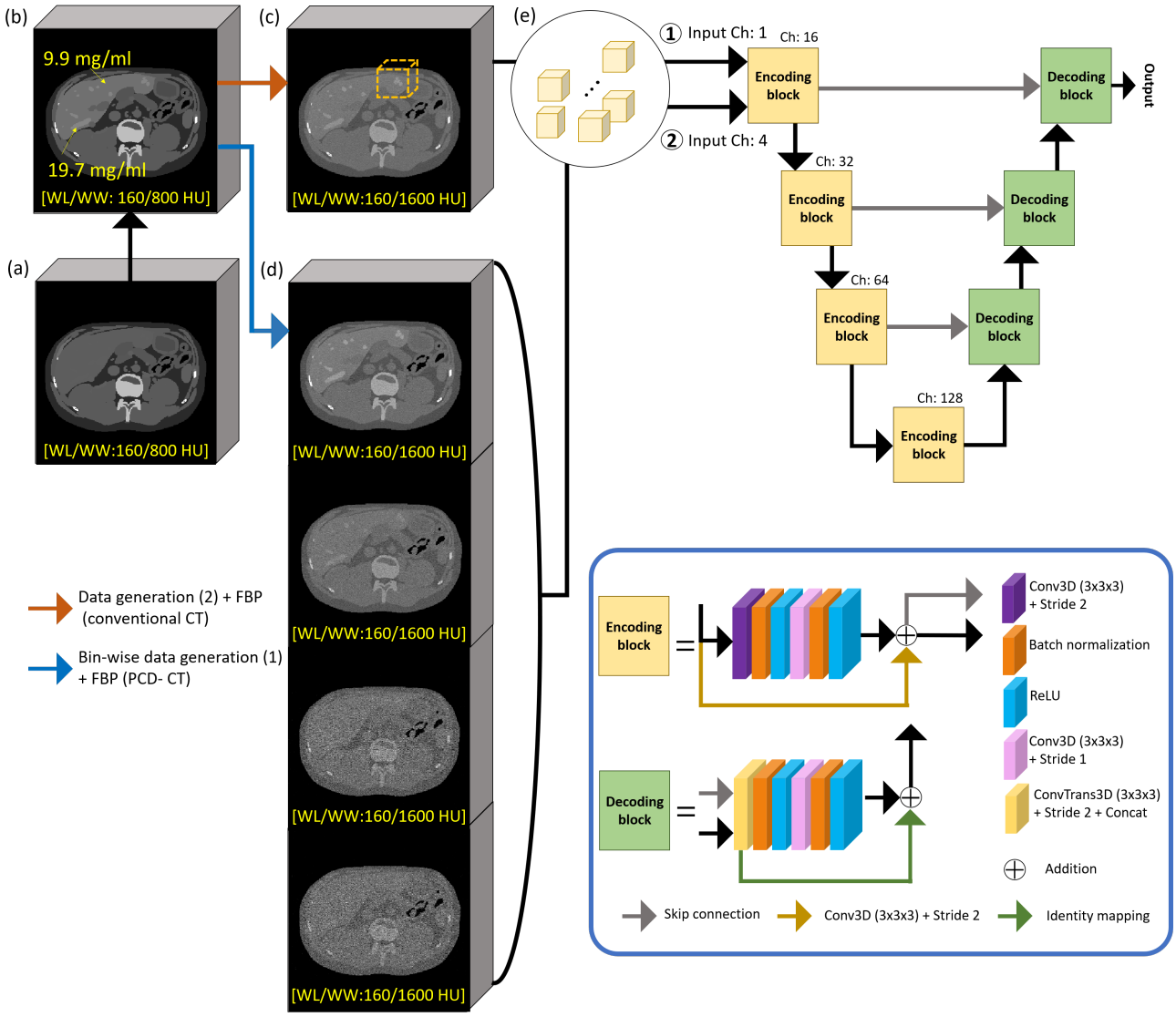

Figure 1. The overview of liver vessel segmentation pipeline using the simulated PCD-CT and conventional CT dataset. (a) 3D volume of the ground truth before the addition of iodine, (b) after the addition of iodine, (c) 3D volume conventional CT data, (d) 3D volume of PCD-CT dataset, and (e) 3D patches randomly extracted from each data.

The spectral distortion is modeled in $S_b(E)$,[10] and water beam hardening correction is applied before we perform the FBP. The number of PCD channels and views are 601 and 1000, respectively, and the ASTRA toolbox is used for the projection and FBP with fan-beam geometry.[12] The distance from the source to the iso-center and the distance from the iso-center to the detector are 500 mm, respectively.

2.2 UNET architecture

We use UNET for both PCD-CT and conventional CT. It is worth noting that UNET for PCD-CT takes 4-channel input unlike the conventional CT one to take advantage of multi-energy information in PCD-CT. The UNET consists of an encoding process and a decoding process. The context of the image is obtained in the encoding process, which is combined with the feature map of the decoding process to enable more accurate localization.[13] As shown in Fig. 1(e), 3D patches are extracted from the 3D volume images of each subject and used for training.

The UNET structure is mainly composed of 3x3x3 convolution filter, and two convolutions are performed for each block. The first layer of the encoding block is convolution with stride 2, reducing the size of the image. The first layer of the decoding block is the transposed convolution with stride 2, and the feature map of the same image size obtained during the encoding process is concatenated by the skip connection process. Starting from the second layer, batch normalization, ReLU, convolution with stride 1, batch normalization, and ReLU are performed in the order. The residual unit is applied to both blocks, 3D convolution with stride 2 is performed in encoding block to reduce the feature size, and then added to the output feature of the encoding block, and the identity mapping is used in the decoding block.[14] The parameters are updated using the softmax function combined with dice loss. We obtain two channel outputs for both PCD-CT and conventional CT, the foreground and background. They are compared pixel-wise to make a binary image.

3. EXPERIMENTS

The experiment is conducted using a total of 56 abdominal simulation phantoms consisting of 33 adult men and 23 adult women.[15] A three-dimensional CT dataset consisting of about 100 slices including the liver region is used, and each slice is generated at 1.5 mm intervals.

As shown in Fig. 1(b), the concentration of iodine in the liver is set to 9.9 mg/ml and the concentration of iodine in the liver vessel is set to 19.7 mg/ml. The iodine concentration is chosen for low dose agents that can clinically reduce the risk of contrast-induced nephropathy, which is a challenging case to segment liver vascular structures.[11]

For UNET training, we generate 150 patches having a size of 64x64x64 pixels for each subject. Thus, the PCD-CT dataset has four input channels in Fig. 1(d), and the conventional CT has one input channel in Fig. 1(c). Our experiment runs on GeForce RTX 3090. We implemented UNET using a MONAI library, a Pytorch-based open-source framework,[16] which consists of 16, 32, 64, and 128 channels, and uses 2 strides and 3x3x3 kernel sizes, and the learning rate was 10^{-3}. The batch size was 1 and the epoch size was 1500. Training dataset, test dataset, and validation dataset were divided into 6:2:2 ratios, and performance was evaluated through 5 fold cross-validation.

3.1 Quantitative assessment

To evaluate the quantitative performance of liver vessel segmentation in PCD-CT and conventional CT, we measure the dice similarity coefficient (DSC). DSC is defined by the following equation:

$$DSC = \frac{2|A \cap B|}{|A| + |B|}, \qquad 0 \leq DSC \leq 1, \tag{3}$$

where A is the segmented (binary) image for each method and B is also a binary image of the ground truth of the target. $|\cdot|$ indicates the number of elements in the set. The more similar the segmented results to ground truth, the higher the DSC value, and the more accurate segmentation is obtained.

The average and standard deviation of DSC scores from 5-fold cross validation on conventional CT and PCD-CT datasets (56 subjects) are reported in Table 1. Overall, DSC scores are under 0.9 because the low

	Conventional CT	PCD-CT
Fold 1	0.861 ± 0.024	0.869 ± 0.025
Fold 2	0.848 ± 0.053	0.860 ± 0.063
Fold 3	0.866 ± 0.024	0.874 ± 0.022
Fold 4	0.839 ± 0.044	0.853 ± 0.041
Fold 5	0.844 ± 0.058	0.858 ± 0.052
Average	0.852 ± 0.042	0.863 ± 0.043

Table 1. The table of dice similarity coefficients for each fold and average of 56 subjects (mean ± standard deviation).

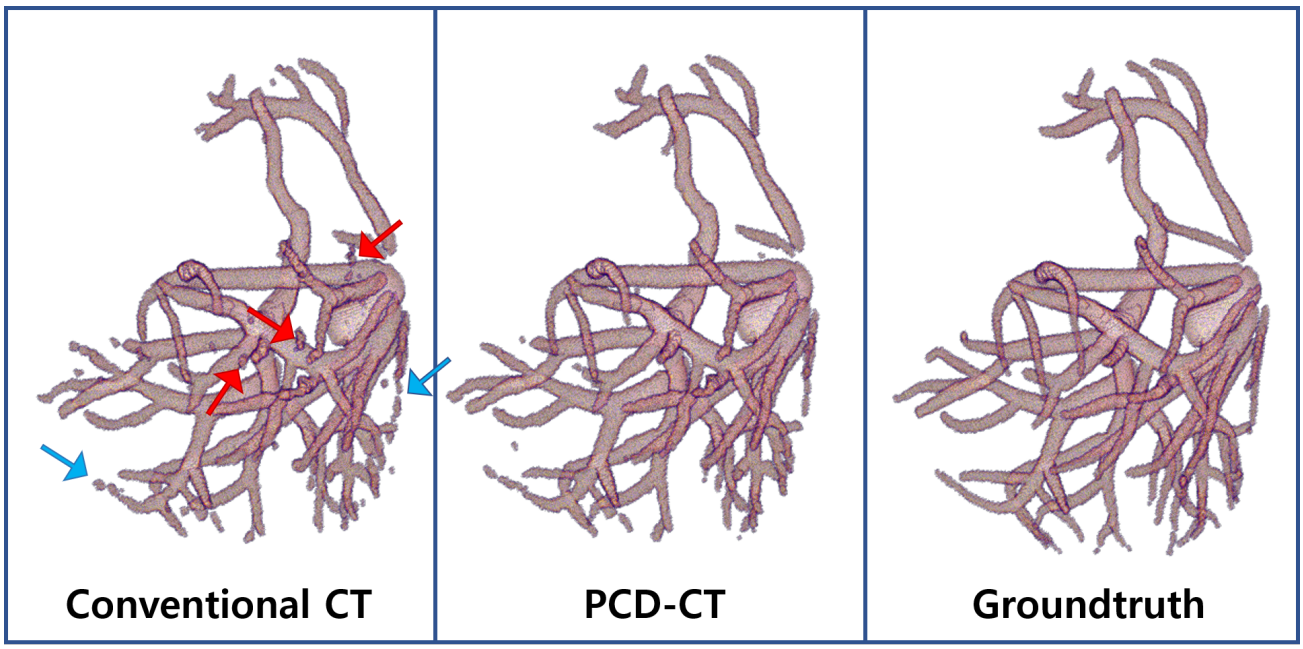

Figure 2. Liver vessel segmentation of the female subject. (red arrow: mis-segmented area, blue arrow: disconnected area)

number of photons and low concentration iodine are used toward the realistic simulation. On average, UNET with PCD-CT significantly improves the DSC by 0.011 (2.6 times of 0.043 standard deviation) compared with UNET of conventional CT. For all folds, PCD-CT shows the consistent improvement of liver vessel segmentation performance over conventional CT. This indicates that PCD-CT enhances the contrast of iodine-injected vascular structures in the liver, benefiting liver vessel segmentation using deep learning.

3.2 Qualitative assessment

For qualitative assessment, we visualize the three-dimensional vascular structure from the UNET-based liver vessel segmentation from both conventional CT and PCD-CT in Fig. 2 and 3. We also show the ground truth vessel structure from the corresponding phantom as reference. We note that each person has a very different appearance and size of vessels, posing the challenge in deep learning segmentation. Compared to the conventional CT, UNET on PCD-CT produces the more accurate segmentation similar to ground truth. In the segmentation results from conventional CT, it is observed that there are disconnected vessels (marked with blue arrow) and false vessel structures (marked with red arrow). This highlights the benefit of using PCD-CT for diagnosing and treating liver disease over conventional CT.

4. CONCLUSION

In this paper, we generated PCD-CT datasets by utilizing the characteristics of energy-discrimination capabilities of PCD-CT, and segmented liver vascular structures by learning them using the deep neural network. The experimental performance was compared and analyzed with those of the conventional CT dataset through dice score and 3D vascular structure visualization. The dice score of the PCD-CT dataset were significantly higher (2.6 times of standard deviation) than that of the conventional CT dataset. For most testing subjects, the incorrect segmentation of the peripheral part of the vessel was reduced using UNET on PCD-CT. This showed that UNET segmentation using PCD-CT outperformed the one using conventional CT, improving diagnosis and management of liver diseases.

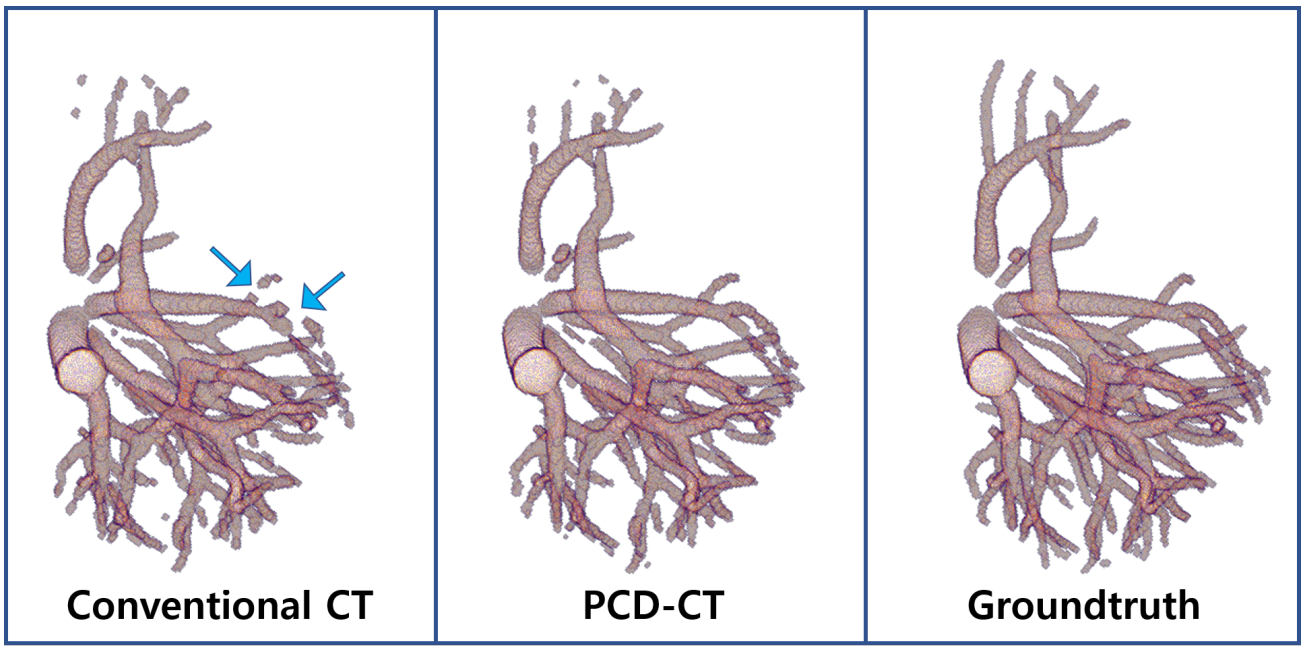

Figure 3. Liver vessel segmentation of the male subject. (blue arrow: disconnected area)

ACKNOWLEDGMENTS

This work was supported by Institute for Information & Communications Technology Promotion(IITP) grant funded by the Korea government (MSIP) (No.2020-0-01524, Development of deep learning-based metal artifact reduction and organ segmentation techniques using spectral CT).

REFERENCES

[1] Conversano, F., Franchini, R., Demitri, C., Massoptier, L., Montagna, F., Maffezzoli, A., Malvasi, A., and Casciaro, S., "Hepatic vessel segmentation for 3d planning of liver surgery: Experimental evaluation of a new fully automatic algorithm," *Academic Radiology* **18**(4), 461–470 (2011).

[2] Fishman, E., Kuszyk, B., Heath, D., Gao, L., and Cabral, B., "Surgical planning for liver resection," *Computer* **29**(1), 64–72 (1996).

[3] Low, G., Wiebe, E., Walji, A., and Bigam, D., "Imaging evaluation of potential donors in living-donor liver transplantation," *Clinical radiology* **63**(2), 136–145 (2008).

[4] Bassignani, M., Fulcher, A., R.A. Szucs, W. C., Prasad, U., and Marcos, A., "Use of imaging for living donor liver transplantation," *Radiographics* **21**(1), 39–52 (2001).

[5] Kaftan, J., Tek, H., and Aach, T., "A two-stage approach for fully automatic segmentation of venous vascular structures in liver CT images," *Medical imaging 2009: image processing* **7259**, 725911 (2009).

[6] Yu, W., Fang, B., Liu, Y., Gao, M., Zheng, S., and Wang, Y., "Liver vessels segmentation based on 3d residual U-NET," *2019 IEEE International Conference on Image Processing* , 250–254 (2019).

[7] Huang, Q., Sun, J., Ding, H., Wang, X., and Wang, G., "Robust liver vessel extraction using 3D U-Net with variant dice loss function," *Computers in biology and medicine* **101**, 153–162 (2018).

[8] Kitrungrotsakul, T., Han, X., Iwamoto, Y., Lin, L., Foruzan, A. H., Xiong, W., and Chen, Y., "Vessel-net: A deep convolutional neural network with multi pathways for robust hepatic vessel segmentation," *Computerized Medical Imaging and Graphics* **75**, 74–83 (2019).

[9] Leng, S., Bruesewitz, M., Tao, S., Rajendran, K., Halaweish, A. F., Campeau, N. G., Fletcher, J. G., and McCollough, C. H., "Photon-counting detector CT: system design and clinical applications of an emerging technology," *Radiographics* **39**(3), 729–743 (2019).

[10] Schlomka, J. P., Roessl, E., Dorscheid, R., Dill, S., Martens, G., Istel, T., Bäumer, C., Herrmann, C., Steadman, R., Zeitler, G., Livne, A., and Proksa, R., "Experimental feasibility of multi-energy photon-counting K-edge imaging in pre-clinical computed tomography," *Phys. Med. Biol.* **53**, 4031–4047 (2008).

[11] Radon, M., Kaduthodil, M., Jagdish, J., Matthews, S., Hill, C., Bull, M., and Morcos, S., "Potentials and limitations of low-concentration contrast medium (150 mg iodine/ml) in CT pulmonary angiography," *Clinical radiology* **66**(1), 43–49 (2011).

[12] van Aarle, W., Palenstijn, W. J., Beenhouwer, J. D., Altantzis, T., Bals, S., Batenburg, K. J., and Sijbers, J., "The ASTRA Toolbox: A platform for advanced algorithm development in electron tomography," **157**, 35–47 (2015).

[13] Ronneberger, O., Fischer, P., and Brox, T., "U-net: Convolutional networks for biomedical image segmentation," 234–241 (2015).

[14] Kerfoot, E., Clough, J., Oksuz, I., Lee, J., King, A., and Schnabel, J., "Left-ventricle quantification using residual u-net," 371–380 (2018).

[15] Segars, W. P., Mahesh, M., Beck, T. J., Frey, E. C., and Tsui, B. M. W., "Realistic CT simulation using the 4D XCAT phantom," *Med. Phys.* **35**, 3800–3808 (Aug. 2008).

[16] Consortium, T. M., "Project monai," (2020).